IOP Publishing and International Atomic Energy Agency Nuclear Fusion
Nucl. Fusion **47** (2007) 667–676 doi:10.1088/0029-5515/47/7/017

Fluctuations and transport in the TCV scrape-off layer

O.E. Garcia[1], J. Horacek[2], R.A. Pitts[3], A.H. Nielsen[1], W. Fundamenski[4], V. Naulin[1] and J. Juul Rasmussen[1]

[1] Association EURATOM–Risø National Laboratory, Technical University of Denmark, OPL-128 Risø, PO Box 49, DK-4000 Roskilde, Denmark
[2] Association EURATOM–Institute of Plasma Physics, Prague, Czech Republic
[3] Ecole Polytechnique Fédérale de Lausanne (EPFL), Centre de Recherches en Physique des Plasmas, Association EURATOM–Confédération Suisse, CH-1015 Lausanne, Switzerland
[4] EURATOM/UKAEA Fusion Association, Culham Science Centre, Abingdon, Oxon OX14 3DB, UK

E-mail: odd.erik.garcia@risoe.dk

Received 25 January 2007, accepted for publication 30 April 2007
Published 27 June 2007
Online at stacks.iop.org/NF/47/667

Abstract
Fluctuations and particle transport in the scrape-off layer of TCV plasmas have been investigated by probe measurements and direct comparison with two-dimensional interchange turbulence simulations at the outer midplane. The experiments demonstrate that with increasing line-averaged core plasma density, the radial particle density profile scale length becomes broader. The particle and radial flux density statistics in the far scrape-off layer exhibit a high degree of statistical similarity with respect to changes in the line-averaged density. The plasma flux onto the main chamber wall at the outer midplane scales linearly with the local particle density, suggesting that the particle flux here can be parameterized in terms of an effective convection velocity. Experimental probe measurements also provide evidence for significant parallel flows in the scrape-off layer caused by ballooning in the transport of particles and heat into the scrape-off layer. The magnitude of this flow estimated from pressure fluctuation statistics is found to compare favourably with the measured flow offset derived by averaging data obtained from flow profiles observed in matched forward and reversed field discharges. An interchange turbulence simulation has been performed for a single, relatively high density case, where comparison between code and experiment has been possible. Good agreement is found for almost all aspects of the experimental measurements, indicating that plasma fluctuations and transport in TCV scrape-off layer plasmas are dominated by radial motion of filamentary structures.

PACS numbers: 52.35.Ra, 52.40.Hf, 52.65.−y

(Some figures in this article are in colour only in the electronic version)

1. Introduction and overview

Transport of particles and heat by collective motions at the boundary of magnetically confined plasmas is an important problem in controlled thermonuclear fusion research [1–5]. Measurements in the scrape-off layer (SOL) of several divertor tokamak experiments have demonstrated a broadening of the radial plasma density profile with increasing line-averaged core plasma particle density, $\bar{n}_e$ [6–10]. As a consequence, plasma particle fluxes may extend to far greater distances in the SOL than expected on the basis of simple particle balance models invoking perpendicular diffusion alone, in which fast parallel transport is expected to deposit the majority of particles and heat leaving the confined plasma in the divertor regions. In turn this may lead to a significant fraction of the core particle outflux recycling predominantly on the main chamber walls, rather than in the divertor volume as intended [6–11]. As the line-averaged plasma density is further increased, the plasma is unstable to a major disruption believed to be caused by radial convective heat transport [12–16].

In all confinement regimes, the SOL plasma is characterized by fluctuation levels of order unity with asymmetric conditional waveforms and skewed and flattened probability distribution functions (PDFs) [17–26]. Fast camera imaging has revealed the presence of localized structures propagating radially outwards in the SOL [27–31]. There is also increasing evidence for the existence of a significant parallel flow component which is driven by ballooning in the radial turbulence driven transport and thus directed from the outboard midplane region towards the divertor

targets [32–36]. Unlike many of the parallel flows related to particle drifts, which do not necessarily lead to net mass transport, this transport-driven flow component may influence particle migration around the machine and is thus an important ingredient to understand with regard to its potential influence on tritium retention in the next generation fusion experiments [37].

This contribution presents an analysis of probe measurements from the outboard midplane region of ohmically heated TCV discharges with varying $\bar{n}_e$. The scale length of the radial particle density profile in the far-SOL will be shown to increase with increasing $\bar{n}_e$. At the highest densities, the profile broadens to encompass the entire SOL characterized by a single scale length. In this region with broad profiles the particle density and fluctuation-induced flux density fluctuations exhibit a high degree of statistical similarity. The radial variation of the relative fluctuation level, skewness and flatness of the particle density fluctuations are the same for all $\bar{n}_e$, increasing radially outwards. Moreover, both particle and flux density PDFs are found to be universal in shape at the SOL–main chamber interface, with positive skewness and flatness moments [38–41].

The time-averaged values of the particle and radial flux densities at the wall radius are both found to increase quadratically with the line-averaged plasma density. As a consequence, the turbulence driven particle flux in the wall region can be parametrized in terms of an effective convection velocity, although there does not seem to be any simple flux parameterization valid at all radial positions in the SOL and for all values of $\bar{n}_e$. Results will also be presented from measurements of time-averaged parallel flows in the SOL of TCV, revealing a significant transport-driven flow component when flow profiles from matched forward and reversed magnetic field directions are averaged. A simple estimate of this flow offset in the SOL from pressure fluctuation statistics is here shown to be in good agreement with the measurements.

The experimental measurements are compared with a two-dimensional interchange turbulence simulation, employing a simple description of open and closed field line regions. The simulation reveals that plasma transport in the SOL is dominated by radial motion of filamentary structures, which appear as blobs in the plane perpendicular to the magnetic field. This is shown to result in broad plasma profiles, large relative fluctuation levels, asymmetric wave forms, skewed and flattened PDFs, and significant transport-driven parallel flows when estimated from pressure fluctuation statistics. Based on the good agreement between the turbulence simulation and experimental measurements across a range of fluctuation statistics, it is concluded that interchange motions are the salient mechanism underlying the collective dynamics observed in the TCV SOL and by inference in the same region of other tokamaks.

This paper is organized as follows. The following section presents a brief overview of the theory for interchange motions of filamentary plasma structures. In section 3 a description of the experimental configuration and probe measurements is given, and in section 4 results are presented from density scan experiments with focus on the radial plasma profiles and fluctuation statistics. An analysis of the fluctuation-induced particle flux is given in section 5, concentrating on flux parameterization and transport scaling. Transport-driven parallel flows are the subject of section 6. Finally, a discussion of the results and conclusions which may be drawn from them are given in section 7. Throughout the paper, experimental results will be compared, where possible, with the same quantities extracted from the turbulence simulation.

2. Interchange motions

Due to the absence of closed magnetic surfaces but strong $\boldsymbol{B}$-field curvature and gradient, interchange motions have long been suspected as the the cause of collective dynamics and anomalous transport in the SOL of magnetically confined plasmas [42–46]. Non-uniformity of the magnetic field gives rise to charge-dependent magnetic guiding center drifts, and thus a net electric current density which may be written [47]

$$\boldsymbol{J}_B = \frac{P}{B}(\nabla \times \boldsymbol{b} + \boldsymbol{b} \times \nabla \ln B), \tag{1}$$

where $\boldsymbol{b}$ is the unit vector along the magnetic field and P is the total plasma pressure. This cross-field current gives rise to charge polarization,

$$\nabla \cdot \boldsymbol{J}_B = \frac{1}{B}(\nabla \times \boldsymbol{b} + \boldsymbol{b} \times \nabla \ln B) \cdot \nabla P, \tag{2}$$

provided there are pressure gradients perpendicular to both the magnetic field and its direction of curvature or inhomogeneity. This charge polarization mechanism leads to radial motion of filamentary plasma structures via the electric drift, $\boldsymbol{V}_E = \boldsymbol{b} \times \nabla\phi/B$, where ϕ is the electrostatic potential [48–53].

Another important contribution to the electric charge continuity equation is the current due to plasma inertia,

$$\boldsymbol{J}_p = \frac{\rho}{B}\boldsymbol{b} \times \left(\frac{\partial}{\partial t} + \boldsymbol{V}_E \cdot \nabla\right) \boldsymbol{V}_E, \tag{3}$$

generally known as the polarization current, where ρ is the plasma mass density. The divergence of the polarization current density yields the rate of change of the electric drift vorticity $\Omega = \boldsymbol{b} \cdot \nabla \times \boldsymbol{V}_E$. These currents may be balanced by an additional current along the magnetic field due to parallel particle motions, $\boldsymbol{J}_\parallel$. In the absence of viscous stresses, the electric charge continuity equation for a quasi-neutral plasma is to lowest order given by

$$\rho\left(\frac{\partial}{\partial t} + \boldsymbol{V}_E \cdot \nabla\right)\Omega + \frac{1}{B}(\nabla \times \boldsymbol{b} + \boldsymbol{b} \times \nabla \ln B) \cdot \nabla P = \nabla \cdot \boldsymbol{J}_\parallel, \tag{4}$$

describing the balance of polarization, magnetic and parallel electric currents, respectively. In the presence of a blob-like structure with size ℓ, the left hand side of the above equation predicts an inertial velocity scaling for the plasma filament given by [52, 53]

$$\frac{V}{C_s} \sim \left(\frac{2\ell}{R}\right)^{1/2}, \tag{5}$$

where R is the magnetic field radius of curvature. For $\ell \approx 1$ cm and $R \approx 1$ m this yields a radial velocity of the order of

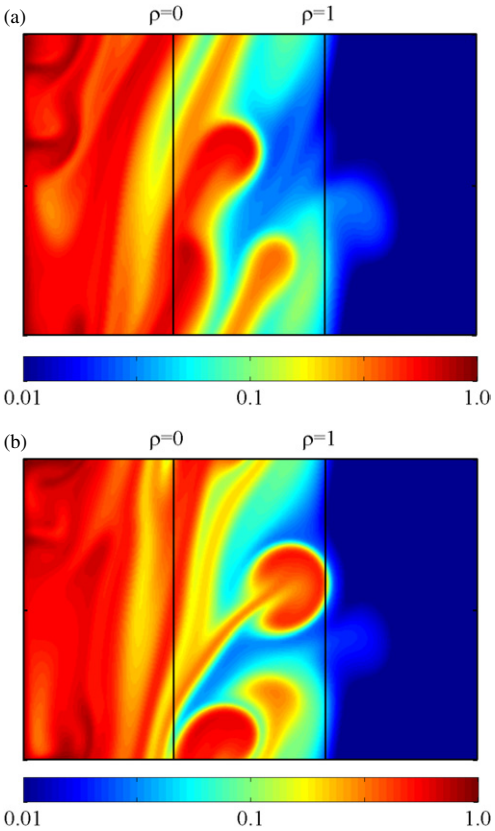

Figure 1. Radial motion of a blob-like structure in the particle density field from the ESEL interchange turbulence simulation. Frame (*a*) is 600 ion gyration periods before frame (*b*). The vertical lines indicate the radial position of the magnetic separatrix and the wall radius.

one-tenth of the acoustic speed C_s. Numerical simulations of the dynamical evolution of isolated blob-like structures have demonstrated rapid acceleration and radial motion over a distance many times the initial structure size. This fast radial motion is accompanied by the development of a steep front and a trailing wake, in agreement with experimental observations [51–55].

A two-dimensional interchange turbulence model, employing a simple description of the open and closed field line regions, has been formulated and implemented in order to describe the collective dynamics in SOL plasmas [56–60]. This model utilizes linear damping terms for all dependent variables as a simple parameterization of the parallel transport of particles, vorticity and heat in the open field line region. The radial localization of this SOL in the simulation domain allows the plasma fluctuations to be driven primarily in the edge region. Numerical simulations using this so-called ESEL interchange turbulence code reveal intermittent eruptions of plasma into the SOL in the form of blob-like structures as presented in figure 1. A description of the model equations and the theory based parameter values can be found in [39], where its predictions were found to agree favourably with electric probe measurements from a high density TCV plasma. Further discussion of the interchange model, and in particular the reason why only the highest TCV density case is simulated, is given in section 7.

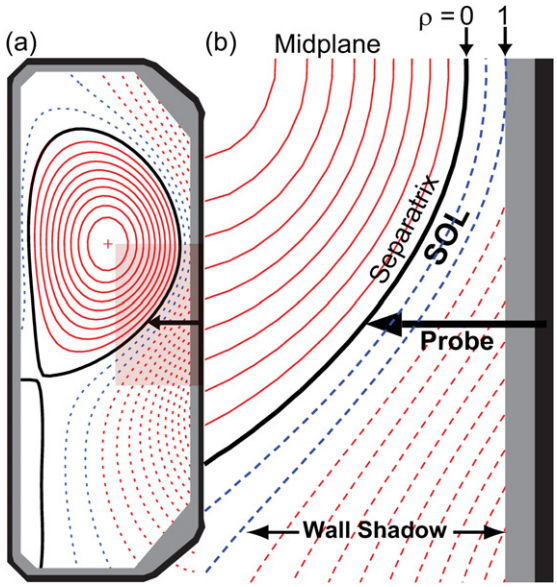

Figure 2. (*a*) Poloidal cross-section of the TCV single null lower diverted configuration. (*b*) Expanded region in the vicinity of the probe reciprocation trajectory, defining the radial coordinate, ρ.

3. Density scan experiments

This paper will be concerned with experimental results from a set of deuterium fuelled, ohmically heated, single null lower diverted TCV pulses with a plasma current of 340 kA, an axial magnetic field of 1.43 T and varying $\bar{n}_e$. The poloidal cross-section of the single null lower magnetic equilibrium is shown in figure 2(*a*), while the expanded region in figure 2(*b*) illustrates the radial trajectory of the fast reciprocating Langmuir probe which is used to obtain the fluctuation measurements. In common with [38–41], a normalized radial coordinate, ρ, is defined, which takes the values 0 and 1, respectively, at the separatrix and wall intersection points of flux surfaces mapped from the probe location to the outside midplane. For these discharges, the midplane wall–separatrix clearance is approximately 3 cm, corresponding to a normalized radial distance of unity.

The probe enters the plasma poloidally approximately halfway between the plasma midplane and X-point for this configuration, thus benefiting from the increased flux expansion there to improve spatial resolution when quantities are mapped to the midplane. The 5-tip Langmuir probe head measures ion saturation current and floating potential at a sampling rate of 6 MHz. A combination of floating potential measurements from two pins separated poloidally by 1 cm yields the poloidal electric field, which is combined with simultaneous measurements of the local fluctuating particle density (at the mid-point between the two floating pins) to estimate the radial turbulence driven particle flux density. For each reciprocation the fluctuation data time series are divided into sub-records of 5 ms, corresponding roughly to a movement of the probe tips of order the 1.5 mm tip length. Since the diagnostic cannot presently measure local temperature fluctuations, they are assumed to be negligibly small when estimating the local particle density from the ion particle flux.

Table 1 lists the TCV pulses considered in the present contribution, their line-averaged densities and the symbols

Table 1. List of TCV density scan experiments, showing the pulse number, the line-averaged core plasma density, $\bar{n}_e$ and the symbols used in subsequent figures.

Pulse number	$\bar{n}_e$ (10^{19} m^{-3})	Symbol
24530	11	▲
26092	8.4	■
26060	6.5	●
26084	4.8	◆
24530	4.4	▼
ESEL	—	○

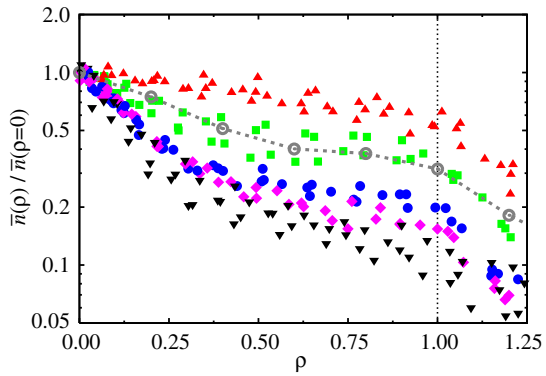

Figure 3. Radial profile of the particle density normalized to the separatrix value. Note that logarithmic scaling is used for the vertical axis.

used in the subsequent figures unless otherwise stated. It should be noted that pulse 24530 is a density ramp discharge, with the first probe reciprocation at a low density, $\bar{n}_e = 4.4 \times 10^{19}$ m^{-3}, and the second at a high density, $\bar{n}_e = 11 \times 10^{19}$ m^{-3}. The latter is close to the density limit for this plasma current and magnetic field configuration. The density ramp experiment was performed with a different probe head compared with that used for the three other pulses in table 1. Due to problems with calibration of the effective probe collecting area, data from this density ramp experiment have been excluded when considering the absolute value of the particle density signal. For a characteristic SOL electron temperature of 20 eV and a parallel connection length $L_\parallel \approx 15$ m, the SOL plasma collisionality, $\nu_e^* = L_\parallel/\lambda_{ei}$, ranges from below 10 to more than 100 in these density scan experiments, where λ_{ei} is the mean free path for electron–ion collisions. The highest density discharge, $\bar{n}_e = 11 \times 10^{19}$ m^{-3}, is the most appropriate to the conditions modelled by the ESEL simulation.

4. Plasma profiles and fluctuations

With increasing $\bar{n}_e$, the time-averaged, radial SOL particle density profile, presented in figure 3, qualitatively changes shape. At low density, the profile has a strong gradient region in the vicinity of the magnetic separatrix, which extends roughly one e-folding length into the SOL. Here the particle density scale length $\lambda_n = -1/(\partial \ln n/\partial r)$ increases from 5 mm to 2 cm as $\bar{n}_e$ increases by a factor of two. Radially outside this so-called near-SOL region, the profiles have a significantly larger scale length, which increases in both magnitude and radial extent with increasing $\bar{n}_e$. In this far-SOL region λ_n increases from 3 cm at the lowest to almost 6 cm at the

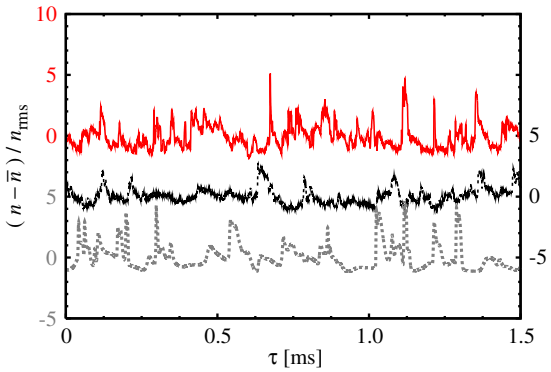

Figure 4. Time series of the particle density at the wall radius from the second (top curve) and first (middle curve) reciprocations of TCV pulse 24530, and from the ESEL interchange turbulence simulation (bottom curve).

highest density, the latter corresponding to an almost flat profile extending from the wall radius to inside the magnetic separatrix. This broadening of the radial plasma profile with $\bar{n}_e$ has been observed in several other tokamak experiments, and is believed to be the cause of the main chamber recycling regime [6–11]. Note that beyond $\rho = 1$, the particle density gradients are much stronger in all cases due to the strong wall sink. Here, magnetic flux tubes connecting to the probe from the high field side first intersect the outboard wall radius with connection lengths of approximately 2 m. On the other side, field lines connect down to the outer target with connection lengths similar to those in the main SOL. Each probe pin thus samples plasma arriving from both high and low field sides along different connection lengths. The net effect on the density outside the wall radius is thus a combination of the two different sink strengths.

Despite significant changes in the time-averaged particle density profiles with increasing $\bar{n}_e$, the plasma fluctuations show a remarkable degree of universality. Figure 4 shows rescaled particle density time series at the wall radius, $\rho = 1$, from the two probe reciprocations of the density ramp TCV pulse number 24530 together with a time series from the ESEL interchange turbulence simulation. These signals clearly have similar features, all three of them characterized by occasional very large fluctuation amplitudes with a steep front and a trailing wake. This bursty nature is even clearer from a conditional average of the particle density time series at the wall radius, presented in figure 5 for all the pulses listed in table 1 together with the interchange turbulence simulation. An amplitude threshold of $n - \bar{n} > 2.5 n_{rms}$ has been used to select conditional sub-records. The average of the conditional signals reveals the same features for all $\bar{n}_e$, namely a strongly asymmetric waveform of roughly 25 μs duration and an amplitude of nearly four times the root-mean-square value of the full time series. Experimentally, the radial electric drift is estimated at approximately 400 m s^{-1}. The structure size based on a simple radial transit is thus about 1 cm, in agreement with the structures seen in the numerical simulation, one example of which is presented in figure 1. Similar estimates have also been reported from other tokamak experiments [20–24].

Figures 6–8 present the radial variation of the relative fluctuation level, the skewness and the flatness of the particle

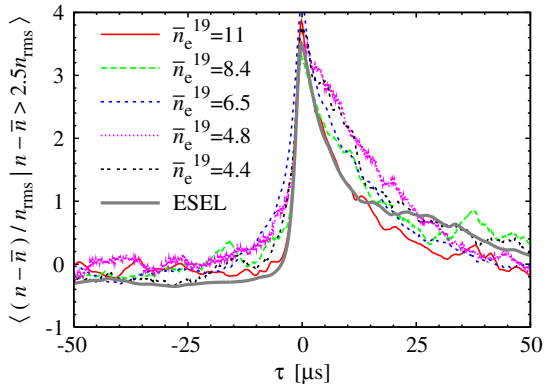

Figure 5. Conditional average of the particle density fluctuations at the wall radius. The line-averaged core plasma density $\bar{n}_e$ is given in factors of 10^{19} m^{-3}.

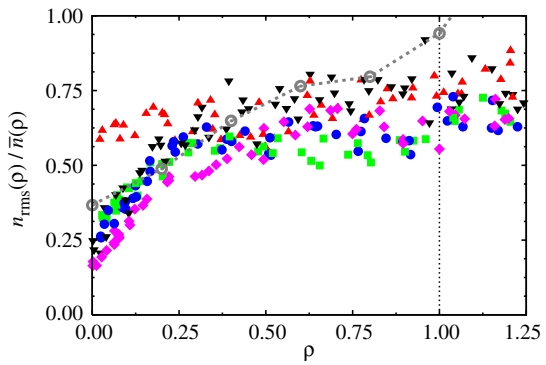

Figure 6. Radial profile of the relative fluctuation level of the particle density.

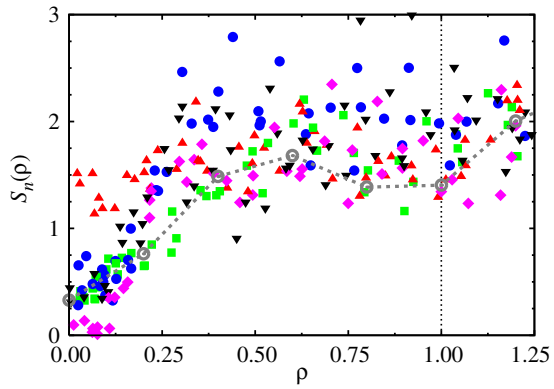

Figure 7. Radial profile of the skewness of the particle density fluctuations.

density fluctuations, the two latter moments defined such as to vanish for a normal distribution. Close to the separatrix the fluctuations are nearly normally distributed, as evidenced by the vanishing skewness and flatness moments for all but the highest density case. In the far-SOL the fluctuations are positively skewed and flattened with a relative fluctuation level of order unity. This simply reflects the abundance of large-amplitude bursts in the time series as seen in figures 4 and 5. Note that the highest density case is characterized by a broad profile and large fluctuations across the entire SOL. Figures 6–8 further show that the relative fluctuation level,

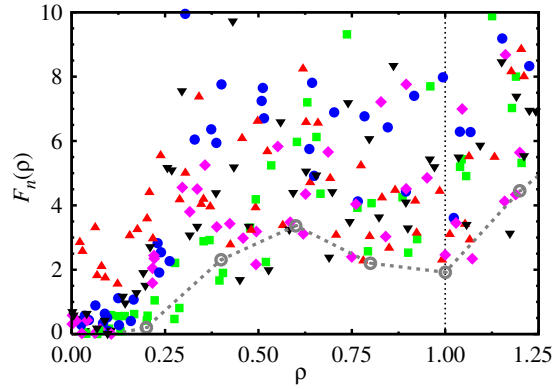

Figure 8. Radial profile of the flatness of the particle density fluctuations.

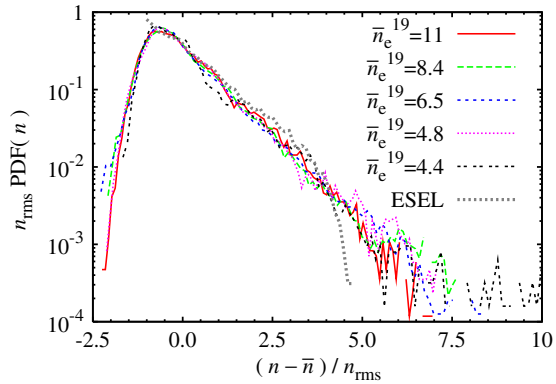

Figure 9. PDF of the particle density fluctuations at the wall radius.

skewness and flatness in the region of broad profiles have the same values and radial shapes for all $\bar{n}_e$, although for the highest moment there is large statistical scatter due to the limited length of the time series. The rescaled PDFs of the normalized particle density fluctuations at the wall radius, $(n - \bar{n})/n_{rms}$, presented in figure 9, collapse to a common shape for all values of $\bar{n}_e$. The distributions are clearly skewed and flattened, with an exponential tail towards large fluctuations. This universality suggests that the mechanism underlying plasma fluctuations in the far-SOL is the same for all values of $\bar{n}_e$.

Treating the turbulence simulation time series in exactly the same way as the experimental time traces yields excellent agreement with regard to the above described statistical parameters. The broad time-averaged radial particle density profile from the simulation agrees with that from the highest density TCV discharges presented in figure 3. Figures 6–8 demonstrate how the profiles of relative fluctuation level, skewness and flatness in the SOL are all well described by the numerical simulation. Moreover, the conditionally averaged wave form and the rescaled PDF of the normalized particle density fluctuations presented in figures 5 and 9 are in excellent agreement with the experimental measurements. This favourable comparison strongly indicates that the commonly observed broad plasma profiles, large relative fluctuation levels, asymmetric fluctuation waveforms, and skewed and flattened PDFs in the far-SOL are due to radial interchange motions of plasma filaments.

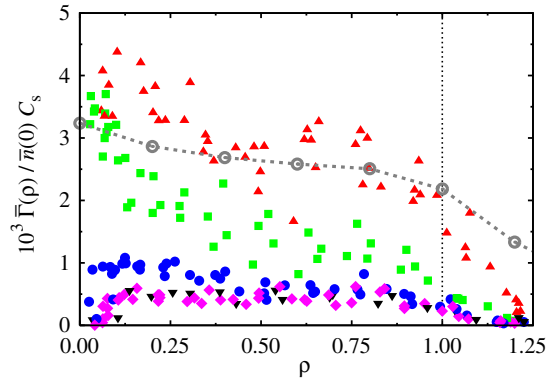

Figure 10. Radial profile of the radial fluctuation-induced particle flux density.

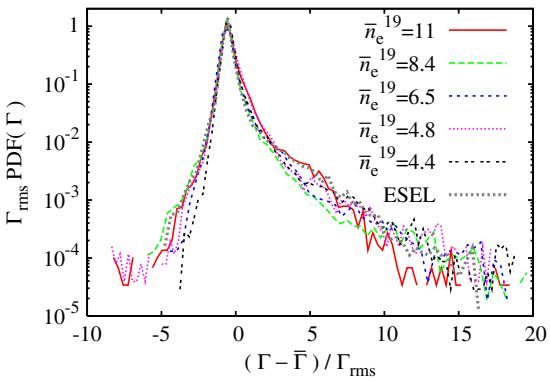

Figure 11. PDF of the radial particle flux density fluctuations at the wall radius.

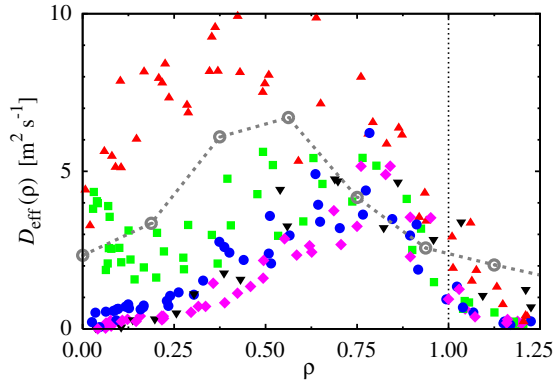

Figure 12. Radial profile of the effective radial diffusion coefficient defined by $\lambda_n\bar{\Gamma}/\bar{n}$.

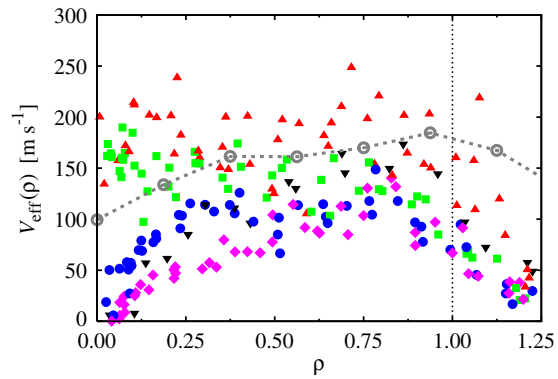

Figure 13. Radial profile of the effective radial convection velocity defined by $\bar{\Gamma}/\bar{n}$.

5. Radial plasma transport

The radial motion of plasma filaments through the SOL clearly has the potential to deposit significant particle fluxes onto the main chamber walls. Figure 10 compiles radial profiles of the fluctuation-induced radial particle flux density, $\Gamma = \tilde{n}\,\tilde{v}_r$, normalized by the product of the particle density at the separatrix and a characteristic acoustic speed of $C_s = 45\,\mathrm{km\,s^{-1}}$. Here $\tilde{v}_r$ is the radial component of the fluctuating electric drift, which in the experiments is estimated from measurements of the floating potential by two probe pins separated poloidally by 1 cm. The associated radial particle flux is the product of this radial velocity and the local ion saturation current fluctuation. The particle flux increases with $\bar{n}_e$ at all radial positions, is roughly constant with ρ at low $\bar{n}_e$ but decreases with radius at the highest $\bar{n}_e$. In common with the wall particle density, the rescaled PDFs of the normalized radial particle flux at the wall radius, $(\Gamma-\bar{\Gamma})/\,\Gamma_{rms}$, presented in figure 11, have a universal shape for all $\bar{n}_e$. This statistical similarity indicates that a common plasma transport mechanism dominates in the far-SOL at all densities.

Fluctuation-induced transport in magnetized plasmas is commonly described in terms of an effective diffusion coefficient, D_{eff}, for the particle flux density, defined by $\bar{\Gamma} = -D_{\mathrm{eff}}\partial\bar{n}/\partial r = \bar{n}D_{\mathrm{eff}}/\lambda_n$ [4–10, 61–65]. The radial variation of D_{eff} estimated from the experimental measurements and the interchange turbulence simulation are presented in figure 12. The experimental D_{eff} generally show a pronounced peak in the outer part of the SOL, which becomes larger and broader with increasing $\bar{n}_e$. Due to this significant variation with radial coordinate and $\bar{n}_e$, the fluctuation-induced particle flux clearly cannot be unambiguously parameterized in terms of an effective diffusivity on the basis of this experimental data. The failure of the diffusion ansatz as a description of experimental measurements, together with the increasing experimental evidence for intermittent SOL transport caused by radial motion of plasma filaments, have motivated the heuristic application of an effective convection velocity, V_{eff}, defined by $\bar{\Gamma} = \bar{n}V_{\mathrm{eff}}$, for parameterization of the particle flux density [5–8, 62–65]. Figure 13 demonstrates that V_{eff} also varies significantly over the radial extent of the TCV SOL at low density. At high density, the effective convection velocity is nearly constant over the SOL. It is interesting to note that in the region with broad particle density profiles, the experimental V_{eff} is roughly the same for all densities.

The broad particle density profile in the SOL at high $\bar{n}_e$, demonstrated in figure 3, leads to large fluxes onto the main chamber wall. In fact, as shown in figure 14, these TCV experiments show that a factor 2 increase in $\bar{n}_e$ yields a factor 4 increase in the time-averaged particle density at the wall radius. The broken line in this figure corresponds to a fitted power law scaling with exponent 1.8 ± 0.3. Using estimates of the fluctuation-induced particle flux from probe measurements, figure 15 presents a similar scaling of the local particle flux density at the wall radius as function of $\bar{n}_e$. The broken line is

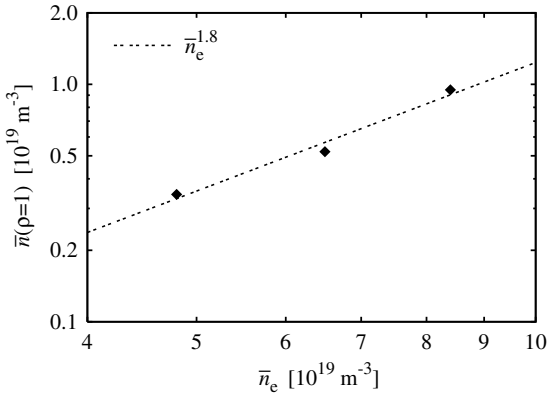

Figure 14. Variation of the particle density at the wall radius with line-averaged density.

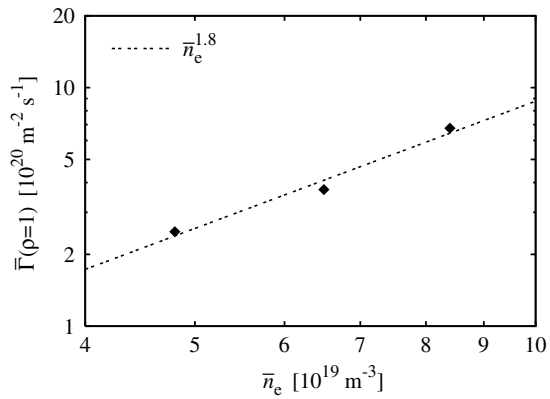

Figure 15. Variation of the radial particle flux density at the wall radius with line-averaged density.

a fitted power law function, again yielding a scaling exponent of 1.8 ± 0.3. For these ohmically heated TCV discharges, there is thus an intimate link between the turbulence driven wall flux and a main operating parameter, namely the line-averaged core plasma density. As mentioned in section 3, data from the density ramp experiment is excluded in this analysis due to calibration problems. The quadratic particle flux scaling with $\bar{n}_e$ found here is consistent with previous investigations on several other tokamak experiments, some of which used particle balance in order to estimate the total ion flux arriving at the main chamber walls [66].

The quadratic scalings of particle and flux densities with $\bar{n}_e$ presented in figures 14 and 15 imply a linear relationship between the local SOL particle and flux densities at the wall radius, as demonstrated in figure 16. This linear relationship in turn suggests that the fluctuation-induced particle flux at the wall radius can be parameterized in terms of an effective convection velocity. A linear fit to the experimental data of the form $\bar{\Gamma}(\rho = 1) = V_{\rm eff}(\rho = 1)\bar{n}(\rho = 1)$, presented by the broken line in figure 16, yields the convective velocity $V_{\rm eff}(\rho = 1) \approx 72\,{\rm m\,s^{-1}}$. This is consistent with the clustering of points at the wall radius seen in figure 13, at least for all but the highest density. The value of the effective convective velocity at the wall radius is evidently related to the radial velocity of filamentary structures. However, it is also influenced by the size distribution and frequency of such transient transport events.

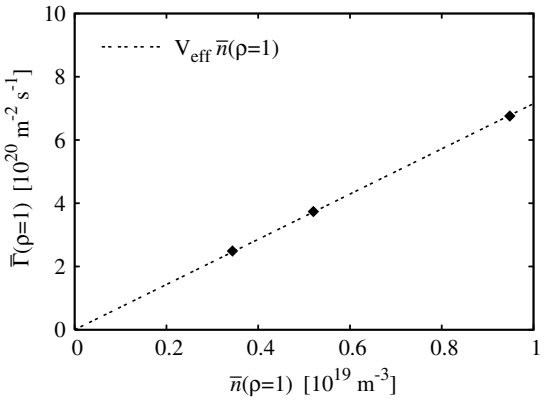

Figure 16. Variation of the radial particle flux density with the particle density at the wall radius.

6. Parallel flows

Mach probe measurements in the SOL of tokamaks with lower or upper single null divertor geometry, double null geometry, and both forward and reversed magnetic fields, have found a significant magnetic field direction independent parallel flow component which is directed poloidally away from the outer midplane [32–34]. One possible explanation for this offset component is a parallel flow driven by radial plasma and heat transport which, due to its ballooning nature, enters the SOL predominantly on the outer midplane. The transient excess plasma pressure caused by the intermittent radial transport at the outboard midplane drains away along field lines, producing a parallel flow towards both the inner and outer divertors in single null geometries.

A dimensionless Mach flow profile is defined by $M_\parallel = V_\parallel / C_s$, where $V_\parallel$ is the parallel fluid flow velocity, and with a positive value defined here as a flow directed towards the outer divertor target. A simple estimate of the time-averaged Mach number that would be expected from these transport-driven flows can be obtained from the product of the sub-sonic value, taken to be approximately 0.5, and the fraction of the time that a significant parallel pressure gradient exists at any radial position, $M_\parallel \approx 0.5 f_{p>\alpha\bar{p}}$ [34, 56, 57]. Here $\bar{p}$ is defined as the local time-averaged pressure, $\triangle t$ is the total duration of the time series, and $t(p > \alpha\bar{p})$ is the time during which the local pressure exceeds the time-averaged value $\bar{p}$ by the factor α. Thus, $f_{p>\alpha\bar{p}} = t(p > \alpha\bar{p})/\triangle t$ is the fraction of time that this condition is satisfied. The radial variation of the inferred parallel Mach number estimated using this ansatz for $\alpha = 1.5$ from the experiments listed in table 1 and the turbulence simulation is presented in figure 17. This figure shows a significant parallel flow whose magnitude is essentially independent of $\bar{n}_e$. Once again, the turbulence simulation is in excellent agreement with the experimental data throughout most of the SOL width.

Transport-driven flows have been investigated on TCV by making Mach probe measurements of parallel SOL flows in a series of discharges with identical magnetic equilibrium at various densities for both forward and reversed toroidal

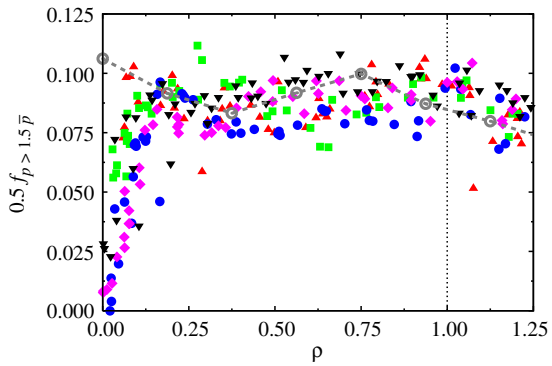

Figure 17. Radial profile of the estimated Mach number from simulation and experiments with plasma current 340 kA.

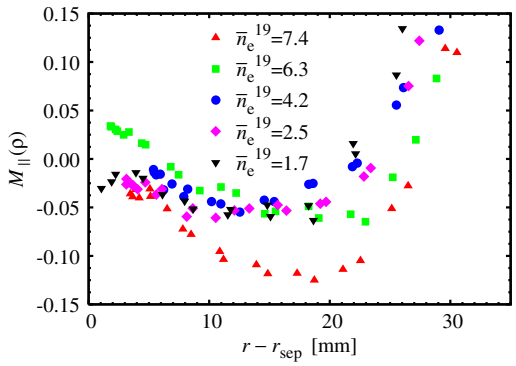

Figure 18. The Mach probe measurements of average parallel flows in the SOL of TCV as function of the mid plane separatrix distance for plasma current 260 kA and $\bar{n}_e$ given in factors of 10^{19} m^{-3}.

field direction [34]. The same single null lower equilibrium is used as for the dedicated turbulence studies described in this paper, and therefore with the probe located 23 cm below the outside midplane. However, a slightly lower plasma current of 260 kA has been chosen to avoid transitions to improved confinement modes, which are easily obtained at higher plasma currents when operating in forward toroidal field. The result is a series of ohmically heated discharge pairs in which plasma conditions are matched as closely as possible, including the SOL profiles of pressure and electric field which are the main components responsible for driving neo-classical drift flows [34].

Figure 18 compiles the averaged radial Mach flow profiles for a range of $\bar{n}_e$, given by 1.7, 2.5, 4.2, 6.3 and 7.4 in factors of 10^{19} m^{-3}. It is re-emphasized that the data used in figure 18 are not taken from the same discharges as used for the other figures in this paper, for which the plasma current was greater by 80 kA. The magnitude of the flow offset is in the range 0.025–0.125 in the central part of the SOL and is in the direction towards the outer divertor target. A flow offset in this direction is what would be expected for a probe located below the outboard midplane region if the flow were driven by ballooning in the radial transport of particles and heat into the SOL. This figure shows a significant parallel flow component which is very similar to that estimated from the pressure fluctuation statistics presented in figure 17 for a slightly higher plasma current.

7. Discussion and conclusions

Due to the presence of ballooning, particles and heat enter the SOL predominantly at the outboard midplane, resulting in parallel pressure gradients in the SOL. For collisionless plasmas, the fast motion of particles along field lines facilitates a regime with plasma filaments being connected to electrostatic sheaths at plasma facing surfaces [48, 49]. The associated sheath currents lead to strong dissipation of plasma fluctuations, and can thus significantly reduce the radial velocity of filamentary structures in the SOL [51, 53]. However, transport of particles and heat along field lines is strongly reduced by particle collisions. Filamentary plasma structures are therefore likely to be effectively disconnected from the sheaths at large plasma collisionality [16, 53]. Due to the diminishing effect of sheath dissipation, there will thus be an increase in the radial velocity of plasma filaments with increasing plasma collisionality [53]. This is consistent with the experimental observations of turbulence driven flux enhancement and broadening of the radial particle density profile with $\bar{n}_e$ reported in sections 4 and 5. The simple parameterization of parallel transport in the ESEL interchange turbulence simulation presented here does not take into account sheath dissipation of the plasma motions [57–60]. This model is therefore unable to describe any transition from sheath connected to disconnected filamentary structures as the plasma density and thus collisionality is increased. For this reason, only simulation results for the highest density case from TCV have been presented here.

In the SOL of ohmically heated TCV plasmas, the radial particle density profile generally has a two-layer structure, with a strong gradient close to the magnetic separatrix, the so-called near-SOL, and a broader part extending radially out to the wall radius, the so-called far-SOL. Both regions have a nearly exponential profile shape, with a characteristic length which increases with $\bar{n}_e$. At the highest attainable plasma density, the far-SOL profile extends all the way to the magnetic separatrix. In the region where the profiles are broad, the particle and turbulence driven flux densities exhibit a high degree of statistical similarity. In particular, the radial variation of the relative fluctuation level, skewness and flatness of the particle density fluctuations are the same for all $\bar{n}_e$ in the discharges studied so far. The fluctuations become stronger and increasingly skewed and flattened outwards in the SOL. This reflects an abundance of large-amplitude bursts in the time series whose structure, revealed by conditional averaging, comprises an asymmetric waveform with a steep front and a trailing wake. Moreover, the rescaled PDFs of the normalized particle and radial fluctuation-induced flux densities at the wall radius are self-similar for all $\bar{n}_e$, with positive skewness and flatness moments.

Most previous theories of turbulence and transport in SOL plasmas have been based on the flux-gradient paradigm, assuming the fluctuations to be driven by local profile gradients [5, 42–46, 61]. On this basis, effective diffusivities have been extensively used to describe radial transport in the SOL [4–10, 62–65]. However, the theoretical foundation for turbulent diffusion involves numerous assumptions, including scale-separation of the passively transported quantity and the existence of a small-scale flow field that is both isotropic

and homogeneous [67–70]. None of these conditions are generally satisfied in the tokamak SOL. It is thus not surprising that the effective diffusivity estimated from the experimental measurements displays strong variations with both radial position and line-averaged density, as shown in section 5. For this reason, an effective convective velocity has often been introduced as an alternative parameterization of the turbulence driven plasma transport [5–8, 62–65]. Although there does not seem to be any simple flux parameterization which is valid through the whole SOL region and for all plasma densities on TCV, a simple convective ansatz shows more robust features, having roughly the same value in the region of broad profiles. At the wall radius position, there is a linear relationship between the local particle and radial flux densities, implying an effective convective velocity of approximately $72\,\mathrm{m\,s^{-1}}$, for all but the highest density ohmically heated TCV plasmas considered here. Both the local particle and flux densities at the wall radius increase quadratically with the line-averaged density, providing a link between a main operating parameter and the turbulence driven wall flux.

A significant transport-driven parallel flow component in the SOL of TCV has been demonstrated by averaging the radial profiles of parallel flow obtained from matched forward and reversed field discharges. Such a flow component has been observed in several other devices and is generally found to be directed from the outer midplane towards the divertor targets. It is thus commonly attributed to ballooning in the radial transport of particles and heat into the SOL. The associated parallel pressure gradients are expected to drive parallel plasma flows directed poloidally away from the outboard midplane. A simple estimate, using pressure fluctuation statistics, of this transport-driven parallel flow component in the TCV SOL is shown here to be in good agreement with experimental measurements. It thus appears that interchange motions due to the unfavourable magnetic curvature at the outboard midplane strongly influences both the radial and parallel transport in the SOL.

Treating the experimental and ESEL simulation time series in the same way reveals excellent agreement in the radial variation of the lowest order statistical moments, temporal correlations, transport-driven parallel flows and the shape of the particle and flux PDFs at the wall radius. The experiments furthermore reveal that in the region with broad radial particle density profiles, the fluctuation statistics remain robust in both magnitude and radial variation with respect to changes in $\bar{n}_e$. On the basis of this favourable agreement between theory and experimental measurement, and the universality found for the latter, it is concluded that fluctuations and transport in the far-SOL are due to radial interchange motions of filamentary plasma structures.

Acknowledgments

The work was partly supported by the Danish Centre for Scientific Computing and by the Swiss National Foundation for Scientific Research. OEG was supported with financial subvention from the Danish Agency for Science, Technology and Innovation. JH was supported by the Grant Agency of the Academy of Sciences of the Czech Republic under grant A100430502 and by INTAS project 05-10000008-8046.

References

[1] Wootton A.J, Carreras B.A., Matsumoto H., McGuire K., Peebles W.A., Ritz Ch.P., Terry P.W. and Zweben S.J. 1990 *Phys. Fluids* B **2** 2879
[2] Wagner F. and Stroth U. 1993 *Plasma Phys. Control. Fusion* **35** 1321
[3] Endler M. 1999 *J. Nucl. Mater.* **266–269** 84
[4] ITER Physics Expert Group on Divertor *et al* 1999 *Nucl. Fusion* **39** 2391
[5] Stangeby P.C. 2002 *Phys. Plasmas* **9** 3489
[6] Lipschultz B., Whyte D. and LaBombard B. 2005 *Plasma Phys. Control. Fusion* **47** 1559
[7] Whyte D.G., Lipschultz B.L., Stangeby P.C., Boedo J., Rudakov D.L., Watkins J.G. and West W.P. 2005 *Plasma Phys. Control. Fusion* **47** 1549
[8] Lipschultz B., LaBombard B., Pitcher C.S. and Boivin R. 2002 *Plasma Phys. Control. Fusion* **44** 733
[9] LaBombard B., Umansky M.V., Boivin R.L., Goetz J.A., Hughes J., Lipschultz B., Mossessian D., Pitcher C.S., Terry J.L. and Alcator Group 2000 *Nucl. Fusion* **40** 2041
[10] LaBombard B., Boivin R.L., Greenwald M., Hughes J., Lipschultz B., Mossessian D., Pitcher C.S., Terry J.L., Zweben S.J. and Alcator Group 2001 *Phys. Plasmas* **8** 2107
[11] Umansky M.V., Krasheninnikov S.I., LaBombard B. and Terry J.L. 1998 *Phys. Plasmas* **5** 3373
[12] Greenwald M. 2002 *Plasma Phys. Control. Fusion* **44** R27
[13] Xu X.Q., Nevins W.M., Rognlien T.D., Bulmer R.H., Greenwald M., Mahdavi A., Pearlstein L.D. and Snyder P. 2003 *Phys. Plasmas* **10** 1773
[14] LaBombard B., Hughes J.W., Mossessian D., Greenwald M., Lipschultz B., Terry J.L. and Alcator C-Mod Team 2005 *Nucl. Fusion* **45** 1658
[15] Antar G.Y., Counsell G. and Ahn S.-W. 2005 *Phys. Plasmas* **12** 082503
[16] D'Ippolito D.A. and Myra J.R. 2006 *Phys. Plasmas* **13** 062503
[17] Heller M.V.A.P., Brasilio Z.A., Caldas I.L., Stöckel J. and Petrzilka J. 1999 *Phys. Plasmas* **6** 846
[18] Sánchez E. *et al* 2000 *Phys. Plasmas* **7** 1408
[19] Antar G.Y., Krasheninnikov S.I., Devynck P., Doerner R.P., Hollann E.M., Boedo J.A., Luckhardt S.C. and Conn R.W. 2001 *Phys. Rev. Lett.* **87** 065001
[20] Boedo J.A. *et al* 2001 *Phys. Plasmas* **8** 4826
[21] Rudakov D.L. *et al* 2002 *Plasma Phys. Control. Fusion* **44** 717
[22] Antar G., Counsell G., Yu Y., Labombard B. and Devynck P. 2003 *Phys. Plasmas* **10** 419
[23] Boedo J.A. *et al* 2003 *Phys. Plasmas* **10** 1670
[24] Kirnev G.S., Budaev V.P., Grashin S.A., Gerasimov E.V. and Khimchenko L.N. 2004 *Plasma Phys. Control. Fusion* **46** 621
[25] Rudakov D.L. *et al* 2005 *Nucl. Fusion* **45** 1589
[26] Xu Y.H., Jachmich S., Weynants R.R. and TEXTOR team 2005 *Plasma Phys. Control. Fusion* **47** 1841
[27] Zweben S.J. *et al* 2002 *Phys. Plasmas* **9** 1981
[28] Zweben S.J. *et al* 2004 *Nucl. Fusion* **44** 134
[29] Terry J.L. *et al* 2005 *Nucl. Fusion* **45** 1321
[30] Grulke O., Terry J.L., LaBombard B. and Zweben S.J. 2006 *Phys. Plasmas* **13** 012306
[31] Myra J.R., D'Ippolito D.A., Stotler D.P., Zweben S.J., LeBlanc B.P., Menard J.E., Maqueda R.J. and Boedo J. 2006 *Phys. Plasmas* **13** 092509
[32] Erents S.K., Pitts R.A., Fundamenski W., Gunn J.P. and Matthews G.F. 2004 *Plasma Phys. Control. Fusion* **46** 1757
[33] LaBombard B. *et al* 2004 *Nucl. Fusion* **44** 1047
[34] Pitts R.A., Horacek J., Fundamenski W., Garcia O.E., Nielsen A.H., Wischmeier M., Naulin V. and Rasmussen J.J. 2007 Parallel SOL flows in TCV *J. Nucl. Mater.* at press
[35] Kirnev G.S., Budaev V.P., Grashin S.A., Khimchenko L.N. and Sarytchev D.V. 2005 *Nucl. Fusion* **45** 459
[36] Terry J.L. *et al* 2003 *Phys. Plasmas* **10** 1739
[37] Pitts R.A. *et al* 2005 *Plasma Phys. Control. Fusion* **47** B303

[38] Garcia O.E., Pitts R.A., Horacek J., Nielsen A.H., Fundamenski W., Graves J.P., Naulin V. and Rasmussen J.J. 2007 Turbulent transport in the TCV SOL *J. Nucl. Mater.* at press
[39] Garcia O.E., Horacek J., Pitts R.A., Nielsen A.H., Fundamenski W., Graves J.P., Naulin V. and Rasmussen J.J. 2006 *Plasma Phys. Control. Fusion* **48** L1
[40] Horacek J., Pitts R.A. and Graves J.P. 2005 *Czech. J. Phys.* **55** 271
[41] Graves J.P., Horacek J., Pitts R.A. and Hopcraft K.I. 2005 *Plasma Phys. Control. Fusion* **47** L1
[42] Nedospasov A.V. 1989 *Sov. J. Plasma Phys.* **15** 659
[43] Garbet X., Laurent L., Roubin J.P. and Samain A. 1991 *Nucl. Fusion* **31** 967
[44] Benkadda S., Garbet X. and Verga S. 1994 *Contrib. Plasma Phys.* **34** 247
[45] Pogutse O., Kerner W., Gribkov V., Bazdenkov S. and Osipenko M. 1994 *Plasma Phys. Control. Fusion* **36** 1963
[46] Sarazin Y. and Ghendrih Ph. 1998 *Phys. Plasmas* **5** 4214
[47] Garcia O.E. 2003 *Eur. J. Phys.* **24** 313
[48] Krasheninnikov S. I. 2001 *Phys. Lett.* A **283** 368
[49] D'Ippolito D. A., Myra J.R. and Krasheninnikov S.I. 2003 *Phys. Plasmas* **9** 222
[50] Garcia O.E., Bian N.H., Naulin V., Nielsen A.H. and Rasmussen J.J. 2005 *Phys. Scr.* **T122** 104
[51] Bian N.H., Paulsen J.V., Benkadda S. and Garcia O.E. 2003 *Phys. Plasmas* **10** 671
[52] Garcia O.E., Bian N.H., Naulin V., Nielsen A.H. and Rasmussen J.J. 2005 *Phys. Plasmas* **12** 090701
[53] Garcia O.E., Bian N.H. and Fundamenski W. 2006 *Phys. Plasmas* **13** 082309
[54] Yu G.Q. and Krasheninnikov S.I. 2003 *Phys. Plasmas* **10** 4413
[55] Aydemir A.Y. 2006 *Phys. Plasmas* **12** 062503
[56] Naulin V., Fundamenski W., Nielsen A.H., Juul Rasmussen J., Garcia O.E., Goncalves B., Hidalgo C., Hron M. and JET-EFDA Contributors Turbulence modeling of JET SOL plasma *Proc. 21st Int. Conf. on Fusion Energy 2006 (Chengdu, 2006)* (Vienna: IAEA) CD-ROM file TH/P6-22 and http://www-pub.iaea.org/MTCD/Meetings/fec2006pp.asp
[57] Fundamenski W., Garcia O.E., Naulin V., Pitts R.A., Nielsen A.H., Rasmussen J.J. and Graves J. 2007 Dissipative processes in interchange driven scrape-off layer turbulence *Nucl. Fusion* **47** 417
[58] Garcia O.E., Naulin V., Nielsen A.H. and Rasmussen J.J. 2006 *Phys. Scr.* **T122** 089
[59] Garcia O.E., Naulin V., Nielsen A.H. and Rasmussen J.J. 2005 *Phys. Plasmas* **12** 062309
[60] Garcia O.E., Naulin V., Nielsen A.H. and Rasmussen J.J. 2004 *Phys. Rev. Lett.* **92** 165003
[61] Connor J.W., Counsell G.F., Erents S.K., Fielding S.J., LaBombard B. and Morel K. 1999 *Nucl. Fusion* **39** 169
[62] Umansky M.V., Krasheninnikov S.I., LaBombard B., Lipschultz B. and Terry J.L. 1999 *Phys. Plasmas* **6** 2791
[63] Pigarov A.Y., Krasheninnikov S.I., Rognlien T.D., Schaffer M.J. and West P.W. 2002 *Phys. Plasmas* **9** 1287
[64] Pigarov A.Yu., Hollmann E.M., Krasheninnikov S.I., Rognlien T.D. and West W.P. 2005 *J. Nucl. Mater.* **337–339** 371
[65] Schneider R., Bonnin X., Borrass K., Coster D.P., Kastelewicz H., Reiter D., Rozhansky V.A. and Braams B.J. 2006 *Contrib. Plasma Phys.* **46** 3
[66] LaBombard B. *et al* 2000 Cross-field transport in the SOL: its relationship to main chamber and divertor neutral control in Alcator C-Mod *Proc. 18th Int. Conf. on Fusion Energy 2000 (Sorrento, 2000)* (Vienna: IAEA) CD-ROM file EX5/6 and http://www.iaea.org/programmes/ripc/physics/fec2000/html/node93.htm#22015
[67] Moffatt H.K. 1983 *Rep. Prog. Phys.* **46** 621
[68] Biferale L., Crisanti A., Vergassola M. and Vulpiani A. 1995 *Phys. Fluids* **7** 2725
[69] Majda A.J. and Kramer P.R. 1999 *Phys. Rep.* **314** 237
[70] Bian N.H. and Garcia O.E. 2005 *Phys. Plasmas* **12** 042307